Oral presentation | Incompressible/compressible/hypersonic flow

Incompressible/compressible/hypersonic flow-II

Wed. Jul 17, 2024 4:30 PM - 6:30 PM Room D

[9-D-01] Characteristics of Mixing and Available Potential Energy Density of Cylindrical Gravity Currents

*Wai Kit Lam[1], Yicheng Cao[1], Leon Chan[1], Duncan Sutherland[2], Richard Manasseh[3], Khalid Moinuddin[4], Andrew Ooi[1] (1. University of Melbourne, 2. University of New South Wales, 3. Swinburne University of Technology, 4. Victoria University)

Keywords: Gravity current, Mixing, Numerical simulation

Twelfth International Conference on Computational Fluid Dynamics (ICCFD12), Kobe, Japan, July 14-19, 2024

Characteristics of Mixing and Available Potential Energy Density of Cylindrical Gravity Currents

W. K. Lam*, Y. Cao*, L. Chan*, D. Sutherland**, R. Manasseh***, K. Moinuddin**** and A. Ooi*
Corresponding author: waikitl@student.unimelb.edu.au * The University of Melbourne, Australia.
** University of New South Wales, Australia.
*** Swinburne University of Technology, Australia.
**** Victoria University, Australia.

Abstract: Direct numerical simulations (DNSs) of three-dimensional cylindrical release gravity currents in a linearly stratified ambient at a Reynolds number of $Re = 3450$ are presented. The investigation focuses on examining the influence of ambient stratification on the dynamics and energy exchange of cylindrical gravity currents across a range of stratification strengths from 0 to 0.8. With increasing stratification strength, the available potential energy (E_a) within the gravity current decreases, resulting in a less energetic flow, particularly notable in strongly stratified cases ($S = 0.8$). During the slumping phase, Kelvin-Helmholtz billows play a crucial role in stirring the heavy fluid and causing irreversible mixing with the ambient fluid. The available potential energy density, $\mathscr{E}_a$, provides spatial maps of local contributions to E_a, offering insights into the interaction between the Kelvin-Helmholtz billows and the current head. This interaction illustrates that increased stratification leads to reduced turbulence and lower available potential energy. Predominantly, significant energy exchanges occur primarily at the top of the billows, with a gradual decrease observed as ambient stratification strength increases.

Keywords: Direct Numerical Simulations, Cylindrical Gravity Current, Stratification, Energy Budget, Mixing, Local Stirring.

1 Introduction

Gravity currents, also referred to as density currents, are a horizontal intrusion of different density ρ_c into an ambient fluid. Gravity currents are observed in many naturally occurring phenomena such as sandstorms [1], powder-snow avalanches [2], and bushfires [3]. Comprehensive reviews of gravity currents in geophysical flows, laboratory experiments, and numerical simulations are given in [4] and [5].

The dynamics of an initially stationary fluid with density ρ_c which is then released into a surrounding medium with density, ρ_0 is examined. The heavy fluid collapses and leads to an intrusion of fluid with a distinct head region. Extensive research has been conducted on the dynamics of gravity currents in both (two-) three-dimensional (3-D) planar and (axisymmetric) cylindrical configurations (without any stratification in the ambient fluid). This research utilises both experimental methods [6, 7, 8] and numerical simulations [9, 10, 11, 12] approaches. These studies have unveiled four distinct stages in the evolution of the gravity current. Initially, after the release of the dense fluid, the gravity current experiences an acceleration phase (the velocity increases from zero to its maximum), during which the gravitational potential energy of the dense fluid is converted into kinetic energy. Once the front velocity reaches its peak, the acceleration phase is succeeded by the slumping phase, characterized by a constant front height and speed.

Following this, the gravity current transitions into the self-similar inertial phase, where the buoyancy force is balanced by the inertial force. Finally, the gravity current enters the viscous phase, in which the viscous force becomes dominant over the buoyancy force. Throughout the inertial and viscous phases, the front velocity of the gravity current decreases according to a power law relationship. It is worth noting that a planar current propagates along a specific direction, where the planform area (the area covered by the gravity current on a horizontal plane) increases linearly with the front location. However, a cylindrical current propagates radially leading to a quadratic increase in the planform area [10]. The diverse characteristics and spreading rates between these two cases give rise to distinct dynamics in gravity currents, influencing their mixing properties.

The presence of stratification in the ambient can significantly alter the propagation and behaviour of gravity currents. Additionally, the presence of stratification leads to the generation of internal waves. The specific layer through which the gravity current propagates depends on the relative strength of the current ($\rho_c^* - \rho_0^*$) and the ambient stratification ($\rho_b^* - \rho_0^*$) ([13, 14]) where ρ_b^*, ρ_0^* and ρ_c^* are the dimensional density at the bottom of the domain, top of the domain and the dense fluid respectively. As a result, numerous experimental and numerical investigations have been conducted to explore the impact of stratification on the dynamics of gravity current. In this regard, Maxworthy *et al.* [13] conducted a comprehensive investigation, utilising both experimental and numerical methodologies to investigate the correlation between the internal Froude number of the gravity current and stratification S in the ambient and

$$S = \frac{\rho_b^* - \rho_0^*}{\rho_c^* - \rho_0^*}. \tag{1}$$

The flow regime of the gravity current flow is determined by the Froude number based on the buoyancy frequency which is a dimensionless parameter defined as the ratio of the inertial forces relative to the gravitational forces, i.e. $Fr = u^*_{f,mean}/N^*H^*$, where $u^*_{f,mean}$ is the mean front velocity in the slumping phase, $N^{*2} = (g^*/\rho_0^*)(-d\rho^*/dz^*) = g^*(\rho_b^* - \rho_0^*)/\rho_0^* H^*$ is the buoyancy frequency, g^* is the gravitational acceleration, ρ^* is the dimensional fluid density, z^* is the vertical coordinate and H^* is the depth of the domain.

Additionally, they presented data of the critical speed, which is defined relative to the linear, mode-one, long internal gravity wave, N^*H^*/π, as well as the location at which the first significant interaction between the wave and the nose of the current was observed. Note that in this manuscript, variables with asterisks ($*$) denote dimensional variables. For the subcritical gravity current ($Fr < 1/\pi$), the internal gravity wave travels faster than the current, whereas for the supercritical gravity current ($Fr > 1/\pi$), the gravity current travels faster than the internal gravity wave.

Early studies concerning the energy budget of gravity currents propagating into an unstratified ambient were carried out by Necker *et al.* [15] and Birman *et al.* [16] using a high-resolution numerical code. Necker *et al.* [15] conducted a comprehensive investigation into the energy budget and mixing behavior of a 3-D, Boussinesq particle-driven gravity current in an unstratified ambient. However, it is noteworthy that the focus of their study differs from the present study. Their finding revealed that approximately 40% of the initial potential energy in the system is ‘lost’ due to particle settling, rendering it unavailable for convective transport and mixing. The particle settling introduces additional dissipative losses in the flow and this a phenomenon not observed in the density-driven gravity currents examined here.

On the other hand, Birman *et al.* [16] analysed the energy budget of a two-dimensional (2-D), non-Boussinesq, lock exchange flow in an unstratified ambient using spectral and compact finite-difference methods. They reported an increase in the rate of conversion of potential energy to kinetic energy with decreasing density ratio $\gamma = \rho_0/\rho_c$. Ungarish and Huppert [17, 18] conducted a study investigating the energy exchange of a 2-D planar and an axisymmetric current at high Reynolds numbers, released from a lock and propagating over a horizontal boundary in both unstratified and linearly stratified ambient. They employed both the shallow-water model and Navier-Stokes finite difference simulations and obtained reasonable agreement in the energy changes of the current between the two approaches. In the case of the axisymmetric current, the energy exchange during the inertial phase was accurately captured using the shallow-water analysis, neglecting the motion in the stratified ambient. The study revealed that stratification enhances the accumulation of potential energy in the ambient and reduces the dissipation of the two-fluid system.

Dai *et al.* [14] conducted experimental and numerical studies on both 2- and 3-D planar release gravity currents in a linearly stratified ambient with varying stratification strength. The energy budgets of the simulations were evaluated by subcritical and supercritical planar gravity currents propagating into a linearly stratified ambient. In the subcritical case, all the energy components showed good agreement between the 2- and 3-D simulations, except for the dissipation rate. For the supercritical case, the 2-D simulations accurately captured the kinetic energy of the current and the potential energy of the ambient are captured but underpredicted the dissipation rate. However, the kinetic energy of the ambient and the potential energy of the current were overpredicted, while the dissipation rate was underpredicted by the 2-D simulations. The discrepancy between the 2- and 3-D simulations for the supercritical case increased dramatically with increasing stratification strength, highlighting the need for cautious interpretation. In conclusion, Dai *et al.* [14] reported that stratification hinders the decay of the total mechanical energy and enhances the accumulation of potential energy in the stratified ambient, which is consistent with the findings of Ungarish and Huppert [17, 18].

Recently, Lam *et al.* [19] conducted 3-D simulations of cylindrical gravity currents propagating into

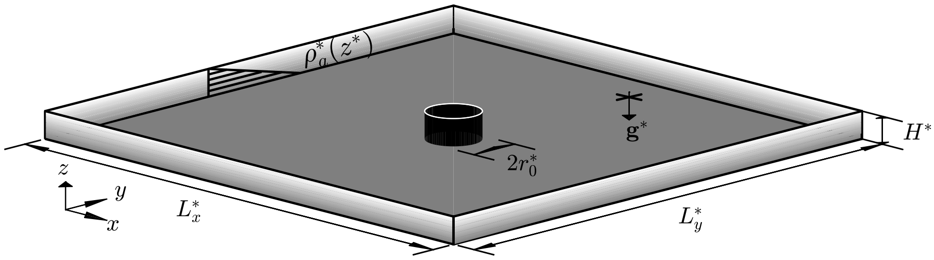

Figure 1: Sketch of the computational domain for the 3-D simulation. The streamwise, spanwise and wall-normal directions are represented by x, y and z, respectively. The cylindrical region of heavy fluid located in the centre of the domain has a density of ρ_c^*. The heavy and ambient fluid has the same height as the height of the domain H^*. The density of the ambient $\rho_a^*(z^*)$ increases linearly from the top ρ_0^* to the bottom boundary ρ_b^* as indicated by the lighter grey shading and the $\rho_a^*(z^*)$ shown on the top left wall.

the stratified ambient fluid with stratification strength that was varied from 0 to 0.8. This analysis aimed to investigate the mixing behaviour of a fully cylindrical gravity current in a stratified ambient at a moderate Reynolds number, employing the mechanical framework proposed by Winters *et al.* [20]. The study unveiled a decrease in both kinetic energy and available potential energy as the current transitioned into a self-similar regime. Notably, both the total potential energy and background potential energy in the stratified cases surpassed those in the unstratified case, attributed to the stratification arrangement in the ambient, which deviates from its equilibrium stable arrangement. During the slumping phase, the irreversible mixing rate was higher for the unstratified case compared to the stratified cases. The results showed the significant role of Kelvin-Helmholtz (K-H) billows in mixing, responsible for stirring the heavy fluid into the current and permanently mixing it with the ambient fluid. In the unstratified case, the flow exhibited higher turbulence compared to stratified cases, with larger K-H billows and a higher local Reynolds number during the slumping phase.

The literature reports on the energy budget of both 2-D and 3-D planar, as well as axisymmetric and cylindrical gravity currents propagating in both unstratified and linearly stratified ambient conditions. While analysing the energy budget aids in understanding the energy exchange between kinetic energy and available potential energy, providing what is known as 'global' statistics, such metrics do not offer insights into the specific locations within the gravity current where stirring and mixing occur. These localised features, termed 'local' stirring and mixing, are the primary focus of our investigation, comparing the characteristics of local energy exchange in a cylindrical current. This study is important because cylindrical currents exhibit different characteristics and dynamics compared to planar currents [10]. Additionally, the presence of stratified ambient can significantly influence the propagation of the current, as indicated in previous studies [21, 22, 23, 14, 24, 25, 26, 27].

This study systematically investigates the effects of stratification strength, S, on the 'local' energy exchange of cylindrical gravity current flow on the horizontal plane, based on the height of the domain and the velocity scale (see equation 7a), at a moderate Reynolds number $Re = 3450$. The choice of this Reynolds number is based on the study conducted by [10], who performed 3-D simulations of cylindrical gravity currents in an unstratified ambient. We describe the formulation of the problem in § 2. In § 3 and 4, we outline the energy budgets and available potential energy density frameworks used to quantify 'global' and 'local' energy exchange. The quantitative results are presented in § 5. Finally, conclusions are drawn in § 6.

2 Computational setup

Figure 1 shows the initial configuration of full-depth cylindrical-release gravity currents in a linearly stratified ambient with $S = 0.5$. The streamwise, spanwise and wall-normal directions are represented by x, y and z, respectively. The computational domain is a square prism with $L_x = L_y = 30$. At time $t = 0$, a cylindrical lock with a unit radius (r_0) and height $H = 1$, containing heavy fluid with density ρ_c is positioned at the centre of the computational domain. The density of the ambient (ρ_a) linearly increases from ρ_0 at the top to ρ_b at the bottom, with $\rho_c > \rho_b$. In the limit of $\rho_b \to \rho_0$ and $S \to \infty$, this becomes the 'classic' case of a gravity current propagating into a homogeneous ambient.

2.1 Numerical method

The 3-D, cylindrical release gravity currents have been simulated using Nek5000, a spectral element, incompressible flow solver [28] with the Boussinesq approximation used to approximate the effects of gravity. Nek5000 has been widely used in various fields [29, 30, 31] due to its high accuracy and scalability in simulating complex flow phenomena. It is hence assumed that the density difference between two fluids is less than 5% [32] to neglect the influence of density differences in the inertial and diffusion terms and retain only in the buoyancy term [33, 34]. The non-dimensional governing equations employed in the study take the form

$$\frac{\partial u_k}{\partial x_k} = 0\,, \tag{2}$$

$$\frac{\partial u_i}{\partial t} + u_k \frac{\partial u_i}{\partial x_k} = \rho e_i^g - \frac{\partial p}{\partial x_i} + \frac{1}{Re}\frac{\partial^2 u_i}{\partial x_k \partial x_k}\,, \tag{3}$$

$$\frac{\partial \rho}{\partial t} + u_k \frac{\partial \rho}{\partial x_k} = \frac{1}{ReSc}\frac{\partial^2 \rho}{\partial x_k \partial x_k}\,, \tag{4}$$

$$\frac{\partial C}{\partial t} + u_k \frac{\partial C}{\partial x_k} = \frac{1}{ReSc}\frac{\partial^2 C}{\partial x_k \partial x_k}\,, \tag{5}$$

where ρ is the density of the fluid, u_i is the velocity for 3-D flow, p is pressure, e_i^g is the unit vector in the direction of gravity and C is the concentration of passive scalar, respectively. The dimensionless density, ρ is defined as

$$\rho = \frac{\rho^* - \rho_0^*}{\rho_c^* - \rho_0^*} \tag{6}$$

where the symbols ρ^*, ρ_0^*, and ρ_c^* with asterisks are the dimensional density of the local, top of the domain and heavy fluid respectively. The tensor notation in equations $2-4$ utilises subscripts i and k, where i represents an unrepeated index (also called a free index) that can take on values $i = 1, 2, 3$, and k represents a repeated index (also known as a dummy index) that signifies a summation over $k = 1, 2, 3$. The value of ρ is bounded between 0 and 1 if $S < 1$. The Schmidt number is $Sc = \nu^*/\kappa^*$ (where ν^* is the kinematic viscosity and κ^* is the molecular diffusivity). Although saline liquid, which is typically used in experiments, has $Sc = 700$, it is found that when Sc is in the order of 1 or larger, there is a weak scaling with the dynamics of the gravity current that does not significantly affect the bulk flow results [35, 15, 10, 36, 37]. It is common practice to set the Schmidt number to unity in numerical simulations of gravity currents, to ensure numerical stability. Therefore, $Sc = 1$ is used in current simulations.

At the bottom ($z = 0$) for the cylindrical release, a no-slip boundary condition is employed, while a slip, impermeable symmetry boundary condition is applied at the top of the domain ($z = H$) and vertical side walls ($x = [-L_x/2, L_x/2]$ and $y = [-L_y/2, L_y/2]$) for the cylindrical release. A zero wall-normal gradient is set for all boundaries for the density field.

The height of the domain H^* is taken as the length scale. The velocity scale, U^*, time scale, T^* and the Reynolds number, Re are defined as

$$U^* = \sqrt{g' H^*}, \tag{7a}$$

$$T^* = \frac{H^*}{U^*}, \tag{7b}$$

$$Re = \frac{U^* H^*}{\nu^*}\,, \tag{7c}$$

where $g' = g^*(\rho_c^* - \rho_0^*)/\rho_0^*$ is the reduced gravity and g^* is the gravitational acceleration acting in the negative z direction. In the ambient, the dimensionless density at the bottom is $\rho_b = (\rho_b^* - \rho_0^*)/(\rho_c^* - \rho_0^*) = S$ where ρ_b^* is the density at the bottom of the ambient and S is the magnitude of the stratification.

The dimensionless density in the ambient ρ_a varies linearly with wall-normal height z from $\rho_a = \rho_b = S$ (where $\rho_a = (\rho_a^* - \rho_0^*)/(\rho_c^* - \rho_0^*)$ and ρ_a^* is density in the ambient) at the bottom ($z = 0$) to $\rho_a = \rho_0 = 0$ at the top ($z = 1$) and

$$\rho_a(z) = S(1 - z), \tag{8}$$

We systematically investigated the local energy exchange for cylindrical gravity currents propagating in an unstratified ambient at a moderate Reynolds number of $Re = 3450$. Subsequently, three stratification strengths of $S = 0.2$, 0.5, and 0.8 were considered and simulated to explore the effect of

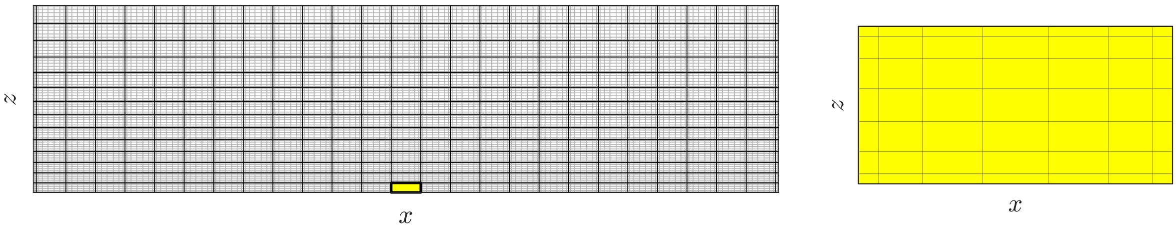

Figure 2: A slice of the mesh for (a) $x-z$ plane with $-2 \leqslant x \leqslant 2$ at $y=0$. The black lines denote the edges of the macro-elements and the grey lines are the GLL nodes within each macro-element. The details of a micro-element are highlighted in the yellow region in (a), as shown in (b).

stratification on the local energy exchange of the cylindrical gravity current. The number of spectral elements employed for cylindrical release simulations are $N_x \times N_y \times N_z = 190 \ \times 190 \ \times 15$. The grid distribution within the spectral element follows the Gauss–Legendre–Lobatto (GLL) grid spacing. A 7th-order polynomial is used in this study and the total number of unique grid points is approximately 1.9×10^8 grid points. Grid stretching (geometrical progression with power coefficient of 1.05) is applied along the wall-normal direction (z) where the grid size at the bottom part is denser than at the top. The topology of the meshes along the $x-z$ plane is shown in Figure 2. The computational grid has a grid spacing of $0.0033 \leqslant \Delta x = \Delta y \leqslant 0.0332$. The grid spacing to Kolmogorov scale ratio, $\Delta l/\eta$ (where $\Delta l = (\Delta x \Delta y \Delta z)^{1/3}$ and η is the Kolmogorov microscale) is calculated at different instantaneous time and is always less than 10. This is more conservative that than the $\Delta l/\eta \approx 16$ recommended by [38] who studied the grid convergence characteristics of spectral element solvers. Therefore, we have ensured that our grid resolution is sufficient to resolve all of the turbulent length scales and also meet the requirement of $\Delta x = \Delta y \approx (ReSc)^{-1/2}$ where $Sc = 1$, see [35, 16, 37]. A variable time step is used to ensure that the Courant number is always less than 0.5.

3 Energy budgets

The energy budget framework proposed by Winters *et al.* [20] is based on the distinction between the adiabatic processes, which allow alterations in initial potential energy without involving heat or mass exchange, and diabatic processes [39]. This approach is independent of distinction between the volume of heavy and ambient fluid, thereby obviating the need to define any interface between the two. This method has been employed in previous studies [40, 41, 42] to analyse 'global' irreversible mixing in stratified flow.

The equation for the time derivative of the kinetic energy (E_k) can be obtained by multiplying the momentum equation (3) by u_i, and has the expression

$$\frac{D}{Dt}\left(\frac{1}{2}u_i u_i\right) = -\frac{\partial}{\partial x_i}(pu_i) + \frac{2}{Re}\frac{\partial}{\partial x_j}(s_{ij}u_i) - \frac{2}{Re}s_{ij}s_{ij} - \rho u_3 \,, \tag{9}$$

where D/Dt denotes the material or convective derivative, s_{ij} is the strain rate tensor where $s_{ij} = \frac{1}{2}(\partial u_i/\partial x_j + \partial u_j/\partial x_i)$ and u_3 is the velocity component in the z direction. The first two terms on the right-hand side of equation (9) are divergence terms, which vanish after integration over the flow domain Ω [15]. Integration of equation (9) over the entire flow domain Ω provides the temporal evolution of the total kinetic energy E_k,

$$\dot{E_k} = \frac{dE_k}{dt} = -\frac{2}{Re}\int_\Omega s_{ij}s_{ij}\ dV - \int_\Omega \rho u_3\ dV \,, \tag{10}$$

$$E_k(t) = \frac{1}{2}\int_\Omega u_i u_i\ dV \,. \tag{11}$$

The potential energy in the system is defined as,

$$E_p(t) = \int_\Omega \rho z\ dV \,. \tag{12}$$

We consider the changes in potential energy of the gravity current flow in a closed system and the time derivative of the potential energy can be determined using equations (4) and (12) [20, 43]

$$\dot{E}_p = \frac{dE_p}{dt} = \int_\Omega \rho u_3 \; dV - \int_\Omega \frac{D\rho}{Dt} z \; dV \,. \tag{13}$$

The first term on the right-hand side of (13) is the vertical buoyancy flux which is reversible rate of exchange with potential energy ($E_k \leftrightharpoons E_p$) and the second term represents a conversion of internal energy to background potential energy due to irreversible diffusion in the density field [20, 14]. Winters *et al.* referred the second term on the right-hand side of equation (13) as $\kappa g A(\Delta\overline{\rho})$ where $\Delta\overline{\rho}$ is the spatial averaging of the density difference between top ($\overline{\rho}(z = H, t)$) and bottom ($\overline{\rho}(z = 0, t)$) over the $x - z$ plane, and $A = L_x L_y$.

The first term on the right-hand side of equation (10) represents the local rate of dissipation ϵ and the time integral of dissipation E_d has an expression

$$E_d(t) = \int_0^t \epsilon(\tau) \; d\tau, \; \epsilon = \frac{2}{Re} \int_\Omega s_{ij} s_{ij} \; dV \,. \tag{14}$$

The summation of equations (10) and (13) gives the change of total mechanical energy with time, $\dot{K} + \dot{E}_p + \int_\Omega (D\rho/Dt) z \; dV = -\epsilon$. In the study by [16], the effect of diffusion in the density field is neglected due to its insignificant role in flows with high Reynolds numbers, where density diffusion can be disregarded in turbulent flows. Integrating the change of total mechanical energy with respect to time yields $E_k + E_p + E_d = \text{const.} = E_k(0) + E_p(0)$ (where $E_k(0)$ is the initial kinetic energy and $E_p(0)$ is the initial potential energy). This essentially represents an energy balance statement during the propagation of the gravity current.

3.1 Partitioning the potential energy

The potential energy of the system can be decomposed into background potential energy E_b and available potential energy E_a. According to Winters *et al.* [20], changes in the potential energy of the background state E_b are direct measure of the energy expended in mixing the fluid. In this context, the constant-density volumes are rearranged, with lighter volumes placed on top of the heavier volumes. The density field undergoes adiabatic rearrangement where the density of the fluid, ρ, increases from the top to the bottom of the domain. This results in redistributed fluid particles within the domain forming a perfectly stable horizontally stratified configuration [20, 42] (see Figure 3.) Adiabatic processes can modify the potential energy but they do not alter the background state $\tilde{\rho}$. Only diabatic mixing can induce changes in the background state in closed systems. The background potential energy is the minimum potential energy attainable through an adiabatic redistribution of ρ and is defined as

$$E_b(t) = \int_\Omega \rho \tilde{z} \; dV \,, \tag{15}$$

where $\tilde{z}(\boldsymbol{x}, t)$ is the vertical position in the reference state of the fluid parcel at position $(\boldsymbol{x}, t)$.

As discussed in [20], the one-dimensional reference profile is defined by

$$\tilde{z}(\boldsymbol{x}, t) = \frac{1}{A} \int H[\rho(\boldsymbol{x}', t) - \rho(\boldsymbol{x}, t)] \; dV' \,, \tag{16}$$

where H is the Heaviside step function satisfying

$$H(\rho(\boldsymbol{x}, t) - \rho_0(\boldsymbol{x}, t)) = \begin{cases} 0, & \rho(\boldsymbol{x}, t) < \rho(\boldsymbol{x}_0, t) \\ \dfrac{1}{2}, & \rho(\boldsymbol{x}, t) = \rho(\boldsymbol{x}_0, t) \\ 1, & \rho(\boldsymbol{x}, t) > \rho(\boldsymbol{x}_0, t) \,. \end{cases} \tag{17}$$

The variable $\tilde{z}(\boldsymbol{x}, t)$ interpreted as a statically stable ordering of the fluid elements, with $\tilde{z}(\boldsymbol{x}_1, t) < \tilde{z}(\boldsymbol{x}_2, t)$ when $\rho(\boldsymbol{x}_1, t) > \rho(\boldsymbol{x}_2, t)$. It maintains the same value across all points on a given isopycnal surface, thus $\tilde{z}$ can be considered a unique function of density ρ [20, 44, 45].

The difference between the potential energy and the background potential energy, namely, the avail-

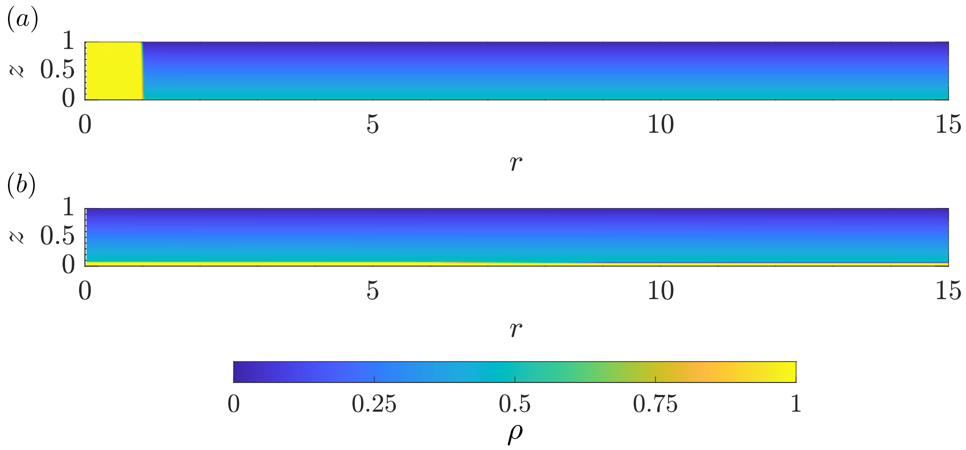

Figure 3: 2-D contour of the azimuthal-averaged density field for the case with $S = 0.5$ in (a) original state and (b) rearranged density field with minimum potential energy state. The heavy fluid is coloured yellow and the density of the ambient $\rho_a(z)$ increases linearly from the top ρ_0 to the bottom boundary ρ_b as indicated by the blue shading.

able potential energy, is expressed as

$$E_a(t) = \int_\Omega \rho(z - \tilde{z}) \; dV = E_p(t) - E_b(t)\,. \tag{18}$$

The available potential energy is the potential energy released in an adiabatic transition from $\rho(z)$ to $\rho(\tilde{z})$ without altering the probability density function of density [20] and is the fraction of potential energy that can be converted to kinetic energy.

4 Available potential energy density

The mechanical energy framework discussed in the previous section provides insight into the overall 'global' energy exchange for cylindrical gravity currents propagating in both unstratified and stratified ambient conditions. However, it does not address the specific locations within the gravity current where the energy exchange occurs, referred to as 'local' energy exchange. The focus of this paper is on the 'local' stirring within the cylindrical release gravity current, where the local energy is available to be converted to kinetic energy (or vice versa). It is important to note that the available potential energy density is not directly related to local 'mixing,' and the stirring process may or may not result in mixing the flow.

Winters and Barkan [46] demonstrated the use of available potential energy density $\mathscr{E}_a$ to construct spatial maps of local contributions to E_a by conducting direct numerical simulations (DNSs) of density stratified flows. The explicit integration of the available potential energy density, $\mathscr{E}_a$ to E_a as provided by Winters *et al.* [20], for Boussinesq fluid flows can be found in the works by Holliday and Mcintyre [47], and Roullet and Klein [48], where

$$E_a(t) = \int \mathscr{E}_a(\boldsymbol{x}, t) \; dV\,, \tag{19a}$$

$$\mathscr{E}_a(\boldsymbol{x}, t) \geqslant 0 \quad \forall \boldsymbol{x}, t\,. \tag{19b}$$

The available potential energy density is defined as,

$$\mathscr{E}_a(\boldsymbol{x}, t) \equiv (z - \tilde{z})(\rho(\boldsymbol{x}, t) - \overline{\rho}(z, \tilde{z}))\,, \tag{20a}$$

$$\overline{\rho}(z, \tilde{z}) = \frac{1}{z - \tilde{z}} \int_{\tilde{z}}^{z} \rho(\tilde{z}') \; d\tilde{z}'\,, \tag{20b}$$

and equation (19a) can then be rewritten as,

$$E_a = \int (z - \tilde{z})\rho(\boldsymbol{x}, t)\ dV - \int \int_{\tilde{z}}^{z} \rho(\tilde{z}')\ d\tilde{z}'\ dV\,. \tag{21}$$

Each parcel with a volume $dV = dxdydz$ is initially 'flattened' to a size $A\ d\tilde{z}$. These flattened parcels, with a thickness of $d\tilde{z} = dV/A \ll dz$, are then stacked in order of descending density (see Figure 3 (b)). In this configuration, $(z_i - \tilde{z}) > 0$, and the average density of the reference profile over the range of heights, $\rho(z_i, \tilde{z})$, is greater than $\tilde{z}(\rho_i)$ and thus must be less than ρ_i. This results in the product in (20a) being positive for all parcels. A detailed explanation of parcel relocation from z_i to $\tilde{z}_i$ in (18) and the mapping of three-dimensional energy equivalents to one-dimensional is discussed in [46].

5 Results and discussion

The discussion will begin with an examination of the propagation and 'global' energy exchange of the cylindrical gravity current, highlighting the impact of stratification strength on its dynamics. The mechanical energy framework introduced by Winters *et al.* [20] will be utilised to calculate the 'global' energy exchange. The focus will be on the available potential energy, which represents the potential energy released in an adiabatic transition from $\rho(z)$ to $\rho(\tilde{z})$ without altering the probability density function of density. This energy fraction indicates the portion of potential energy that can be converted to kinetic energy.

In the subsequent section, the available potential energy density, $\mathscr{E}_a$, as introduced by Winters and Barkan [46], will be employed to construct spatial maps of local contributions to E_a. This approach will allow for exploration of the reversible stirring process ($E_k \rightleftharpoons E_a$) within the cylindrical gravity current propagating in stratified ambient. It should be emphasised that the mixing discussed in the sections below referred to as 'global' mixing.

5.1 Propagation and 'global' energy exchange of cylindrical gravity current with different stratification

The time series of the propagation of the cylindrical gravity current in both $S = 0$ (left column) and 0.5 (right column) can be visualised in Figure 4. The heavy fluid is coloured yellow and the stratified ambient $S = 0$ is represented by blue, and linearly stratified ambient is indicated by blue shading. The solid black lines in Figure 4($f - j$) represent the isopycnals. The red vertical lines indicate the front location of the current and white arrows represent the Kelvin-Helmholtz billows.

At an early time ($t = 1$), the heavy fluid slumps into the ambient fluid, showing no significant difference between the cases. During the slumping phase, between $3 < t < 5$, K-H billows form behind the current head at $t = 3$ for the unstratified case, while for $S = 0.5$, these billows form at $t = 5$. At this time ($t = 5$), the current in the unstratified case travels a significantly greater distance than in the $S = 0.5$ case. This indicates that stratification hinders the propagation of the gravity current, delays vortex formation, and results in less turbulence [14, 26].

Interestingly, at $t = 7$ and $t = 9$ (see Figure 4(i) and (j)), when the current is in the inertial phase, the $S = 0.5$ case exhibits a similar density contour to the unstratified case at $t = 5$ and $t = 7$ (refer to Figure 4(c) and (d)), indicating that the development of the Kelvin-Helmholtz billows is delayed by approximately 2 time units. At $t = 9$, the merging of the K-H billows with the head of the gravity current is observed for the unstratified case. However, for $S = 0.5$, the K-H billows do not merge with the head (not shown here) but begin to separate from it. This occurs because the gravity current transitions into subcritical flow, where the internal gravity waves separate from the current head, move upstream faster than the current, and prevent the merging of the billows with the head [13, 26]. These figures illustrate the contribution of the K-H billows to the evolution of the available potential energy E_a and the background potential energy E_b, which will be discussed in the following sections.

Examining the energy budget of the cylindrical current in both unstratified and stratified ambient conditions demonstrates the conversion process from available potential energy to kinetic energy. A comparison is made between the unstratified case and the stratified cases with $S = 0.2$, 0.5, and 0.8, which highlights the impact of stratification on the energy exchange of the cylindrical gravity current. The initial available potential energy, $E_a(0)$ is the maximum energy available for conversion to kinetic energy; therefore, all potential energy terms and kinetic energy are normalised with the initial available potential energy.

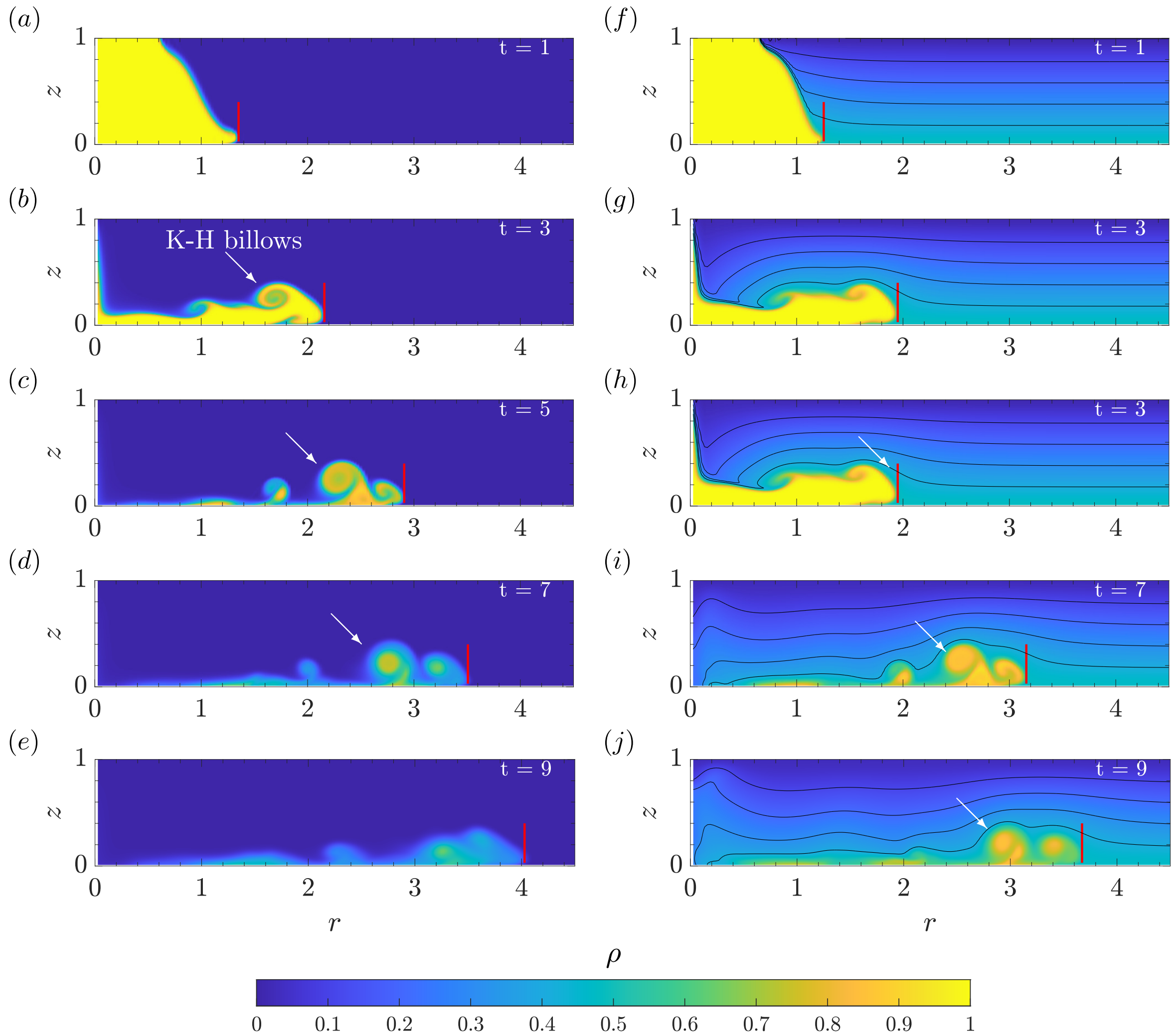

Figure 4: Time evolution of the azimuthal-averaged gravity current in the stratified ambient with $S = 0$ (left column) and 0.5 (right column). Contours are shown with time intervals of 2 time units. The heavy fluid is coloured yellow and the density of the ambient $\rho_a(z)$ increases linearly from the top ρ_0 to the bottom boundary ρ_b as indicated by the blue shading. The solid black line represents the isopycnals. The red vertical lines indicate the front position of the gravity current. The white arrows represent the Kelvin-Helmholtz billows behind the gravity current head.

The temporal evolution of front velocity, u_f, with varying S and the non-dimensional potential energy budget of the gravity current propagating in the unstratified ambient ($S = 0$) at $Re = 3450$ is illustrated in Figure 5. The transition of the gravity current for the $S = 0$ case through different phases is shown in Figure 5(a). The evolution of the potential energies is depicted in Figure 5(b).

At $t = 0$, when the fluid is stationary with no kinetic energy, the total energy is stored as potential energy. The non-dimensional available potential energy, E_a, is approximately 1, indicating that the potential energy is entirely attributable to the conversion to kinetic energy [39]. The non-dimensional background potential energy in Figure 5(b) is small but not zero.

During the initial acceleration phase ($0 < t \leqslant 2.5$) after the heavy fluid is released into the ambient fluid (see Figure 4(a)), both E_p and E_a decrease rapidly, reaching nearly the same value. Background potential energy, E_b, remains close to zero, demonstrating the conversion from potential energy to kinetic energy. This indicates E_p is entirely attributable to the conversion to kinetic energy.

As the current transitions into the slumping phase ($2 < t < 5$), the speed of the current becomes nearly constant (refer to Figure 5(a)) and Kelvin-Helmholtz billows form behind the current head. During this phase, E_a shows a slight increase from a trough (see the black arrow in Figure 5(b)). This indicates reversible stirring of the heavy fluid into the body of the current and irreversible mixing with the ambient

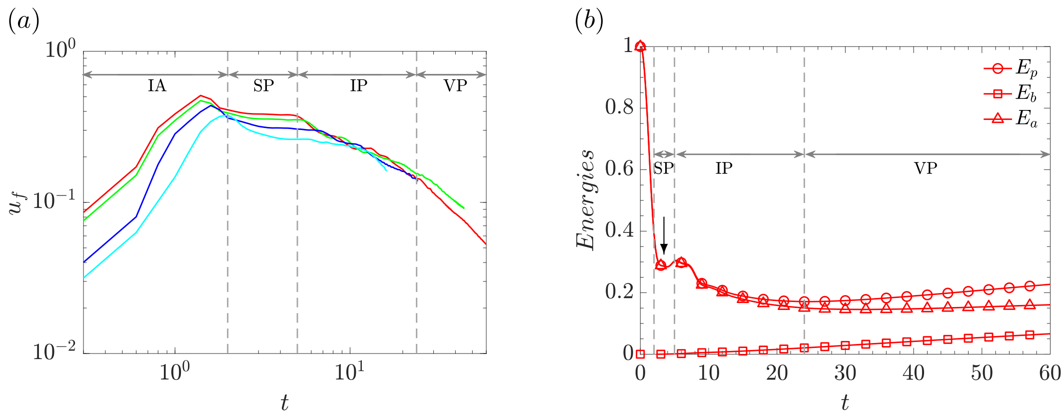

Figure 5: The plot of (a) front velocity against time with different S and (b) non-dimensional potential energies. Total potential energy P, ($\circ$); background potential energy P_b, ($\square$) and available potential energy P_a, ($\triangle$). The transition of the current label in (a) is for $S = 0$ case, IA: initial acceleration and deceleration; SP: slumping phase; IP: inertial phase and VP: viscous phase. The colours in (a) represent different stratification strength, —, $S = 0$; —, $S = 0.2$; —, $S = 0.5$ and —, $S = 0.8$.

fluid caused by K-H billows [39] (see Figure 4(b, c)). Although the value of E_b is low, the increase in E_b reflects the presence of non-zero irreversible mixing, where the trapping of ambient fluid due to K-H billows alters the potential energy and slightly changes the background potential energy [39].

As the current transitions into the self-similar inertial phase, E_p and E_a continue to decrease until approximately $t \approx 24$, while E_b continues to increase as the current propagates. During this phase, E_a gradually separates from the curve of E_p, indicating that the variation of E_p is caused more by the irreversible mixing of fluid elements than by reversible stirring ($E_a \leftrightharpoons K$). This can be seen in Figure 4(d, e)) where the K-H billows are merging with the head of the gravity current, and irreversible mixing is greater than reversible stirring at the time, $7 \leqslant t \leqslant 9$.

At later times ($t > 24$), the current enters the self-similar viscous phase where the viscous force dominates the buoyancy force, resulting in a rapid decay of the current's speed. Interestingly, both E_p and E_a begin to increase, with E_p growing at a higher rate until the end of the simulation. During the viscous phase, the increase in E_p is mainly attributed to laminar diffusive processes rather than the transfer from kinetic energy to available potential energy.

Finally, when $t > 40$, the propagation of the current becomes negligible as there is insufficient density difference between the current and ambient at the bottom wall to continue propagating. The increase in E_a, may be attributed to the presence of fluid with greater density than the ambient density remaining almost stationary within the tail of the gravity current.

Figure 6(a) and (b) show the temporal evolution of normalized available potential energy, E_a and kinetic energy, E_k, as a function of time with S varying from 0 to 0.8 at $Re = 3450$. Kinetic energy is normalized by the initial available potential energy $E_a(0)$, which the sole source of energy available for the stirring process.

Initially, the heavy fluid is stationary, and $E_p = E_a$ and $E_k = 0$. When the simulation starts and the heavy fluid is released and slumps into the ambient, kinetic energy undergoes a rapid increases owing to its conversion from available potential energy. In Figure 6(b), all cases exhibit a similar peak normalized kinetic energy, approximately $E_k \approx 0.65$, occurring between $2.6 < t < 3$. This suggests that around 65% of the initial available potential energy $E_a(0)$ is converted to kinetic energy regardless of the stratification strength of the ambient. It is important to note that $E_a(0)$ increases with increasing S, as reported and illustrated in Figure 6(e) of [19]. Kinetic energy attains its maximum and E_a reaches a local minimum concurrently, just before the gravity current transitions into the slumping phase, characterized by the front velocity reaching an almost constant value.

During the slumping phase, the decreases in E_k and the increase in E_a demonstrate the formation of Kelvin-Helmholtz billows, which contribute to the reversible stirring of the dense fluid into the body of the current. Subsequently, as the current transitions into the inertial phase, characterized by a power-law decay in the front velocity, kinetic energy decreases, resulting in a less energetic current. It is worth noting that E_k depicts higher values with increasing S, due to normalization with $E_a(0)$ where $E_a(0)$ decreases with increasing S.

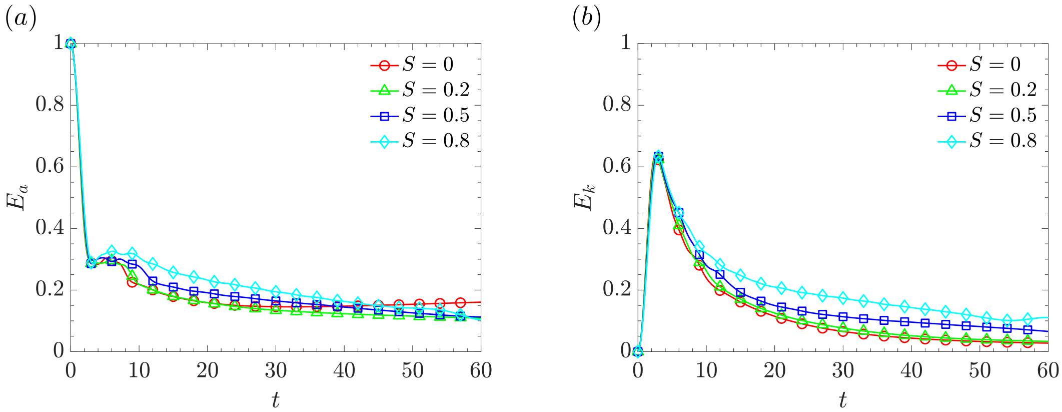

Figure 6: The plot of (a) available potential energy and (b) kinetic energy against time with different S. The colour represents different stratification strength, —, $S = 0$; —, $S = 0.2$; —, $S = 0.5$ and —, $S = 0.8$.

In general, both the kinetic energy and available potential energy in the system decrease with increasing S. This observation implies that the potential energy available for conversion into kinetic energy is influenced by the degree of stratification. This is consistent with the observations reported in [14, 19], where the stratification in the ambient can hinder the release of potential energy associated with the current, which aligns with the result of E_a in Figure 6(a).

5.2 'Local' energy exchange: Available potential energy density, $\mathscr{E}_a$

The energy budgets indicate that as stratification strength increases, the potential energy available for conversion into kinetic energy decreases. During the slumping phase, Kelvin-Helmholtz (K-H) billows form behind the current head, causing reversible stirring of the dense fluid into the body of the current and permanent mixing with the ambient fluid. While K-H billows form and interact with the head of the gravity current in the time range $3 \leqslant t \leqslant 10$, this section will focus solely on the 'local' energy exchange (reversible stirring, $K \leftrightharpoons E_a$) during this period for cylindrical gravity currents propagating in a linearly stratified ambient with varying stratification. Analyzing the spatial distribution of $\mathscr{E}_a$ provides insight into identifying the local contribution of E_a within the gravity current under the effect of stratification. It is important to note that the volume integral of $\mathscr{E}_a$ yields the same E_a as in Figure 6.

Figure 7 illustrates the isosurface of available potential energy density, $\mathscr{E}_a$. The isosurface of density, $\rho = 0.015$, is plotted on top of the isosurface of $\mathscr{E}_a$. The azimuthal-averaged density contour is depicted on the right-hand side. As in Figure 4, the yellow colour represents the heavy fluid, while the unstratified ambient ($S = 0$) is represented by blue, and the linearly stratified ambient is indicated by blue shading. The red solid line represents the front position of the gravity current, and the white arrow indicates the K-H billows. The solid black line represents the isopycnals.

At $t = 3$ (refer to Figure 7(a)), the gravity current transitions into the slumping phase, during which the K-H billows form behind the current head. The value of $\mathscr{E}_a$ is significantly higher at the top part of the billow compared to other regions, indicating that most of the potential energy is concentrated there and is ready to be converted into kinetic energy through the stirring process. This process draws the heavy fluid into the head and body of the current and permanently mixes it with the ambient fluid. The value of $\mathscr{E}_a$ gradually decreases to approximately 0.15 in the body of the gravity current. The motion of the current's tail is minimal, resulting in the lowest available potential energy ($0 < x \leqslant 1$), which does not contribute to the stirring process.

The gravity current begins to transition into the self-similar inertial phase at $t \approx 6$. The azimuthal-averaged density contour shows that the billows behind the current head are significantly larger than the head itself. At this time, the K-H billows appear to be separated from the head, and the density within the billows is higher than in the head. Interestingly, $\mathscr{E}_a$ is higher in the billows, as shown on the isosurface of (E_a located on the left-hand side of Figure 7(b). This indicates that most of the available potential energy is contributed by the K-H billows compared to the vortices within the head. It is also worth noting that the lobes-and-clefts structures are developing at the front of the gravity current and appear symmetrical.

As the gravity current continues to propagate, the lobes-and-clefts structures on the advancing front can be observed clearly in Figure 7(c). The formation of these lobes and clefts instabilities has been reported in [49, 35, 11, 50, 26]. At this time, $t = 9$, the available potential energy density, $\mathscr{E}_a$, within the head becomes higher than in the billows indicating that the vortices within the head have higher E_a resulting in dominant stirring. Consequently, the billows behind the current begin to merge with the head, as shown in Figure 7(c).

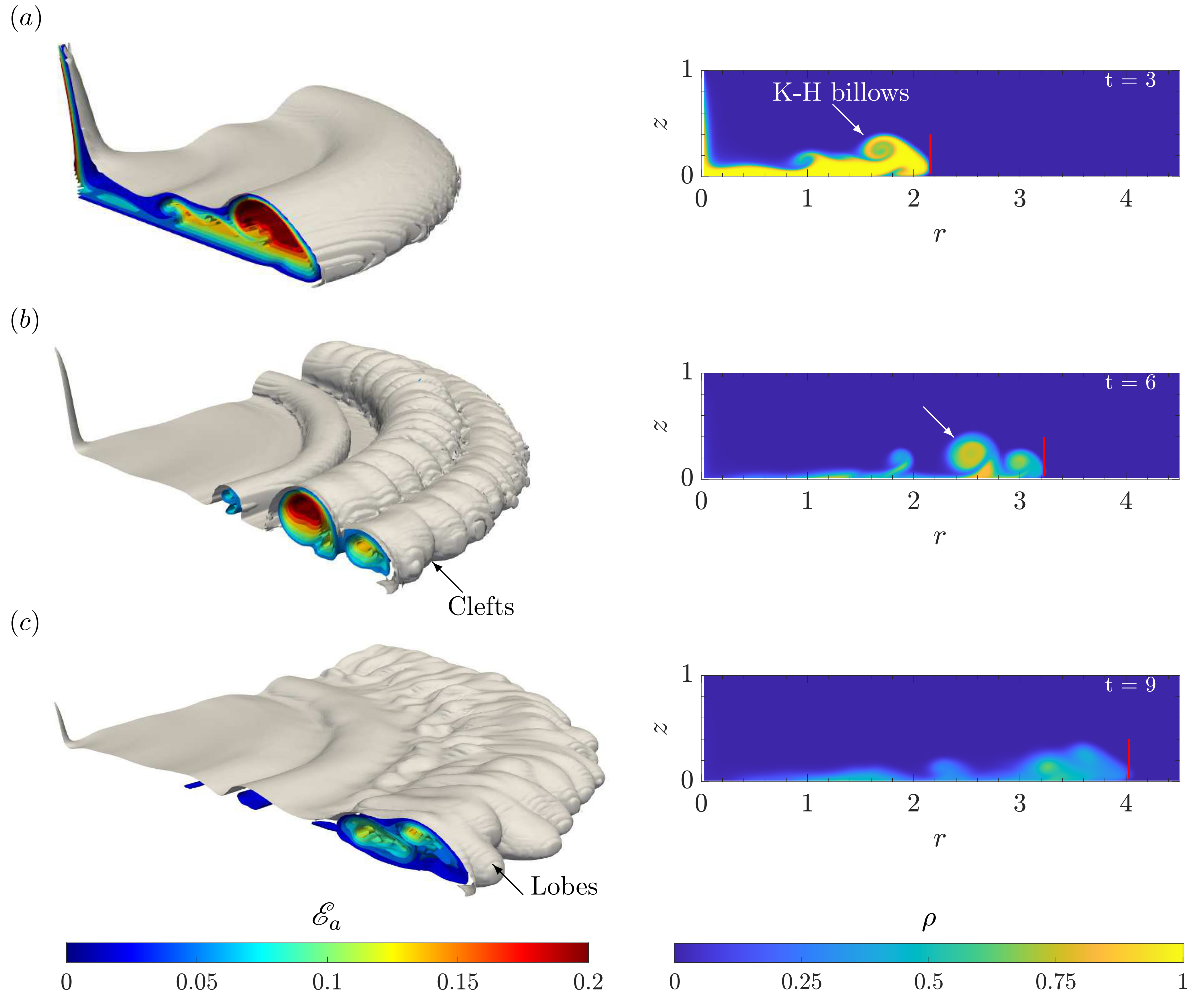

Figure 7: (Caption next page.)

The isosurface of $\mathscr{E}_a$ for cylindrical gravity currents propagating in a stratified ambient with different S values is shown in Figure 7$(d)-(h)$. For the weakly stratified case, $S = 0.2$, the isosurface of $\mathscr{E}_a$ and the azimuthal-averaged density contour (see Figure 7$(d)-(e)$) do not differ significantly compared to the unstratified case. A similar observation of the merging of K-H billows with the current head is observed for $S = 0.2$ at $t = 10$. It is important to note that although the structures do not differ significantly, the delayed formation of K-H billows and their merging with the head are observed in the weakly stratified case, occurring approximately one dimensionless time unit later.

As the stratification strength increases to $S = 0.5$, the structures of the isosurface of $\mathscr{E}_a$ and the contour of azimuthal-averaged density begin to differ compared to the unstratified case. In this scenario, the development of the Kelvin-Helmholtz billows (refer to Figure 7(f))is delayed by approximately two dimensionless time units compared to the unstratified case shown in Figure 7(a). The available potential energy density within the current head is significantly smaller compared to the $S = 0$ and $S = 0.2$ cases. The radially advancing lobes and clefts of the current become smaller, with the mean wavelength of the lobes decreasing as the stratification strength increases [26]. The structures behind the current are also different compared to the $S = 0$ and $S = 0.2$ cases, with the tail separating from the current as observed at $r < 1.4$ in Figure 7(f).

At a later time, $t = 10$, as shown in Figure 7(g), the K-H billows do not merge with the current head but continue to propagate downstream behind it. This is attributed to the effect of stratification, where

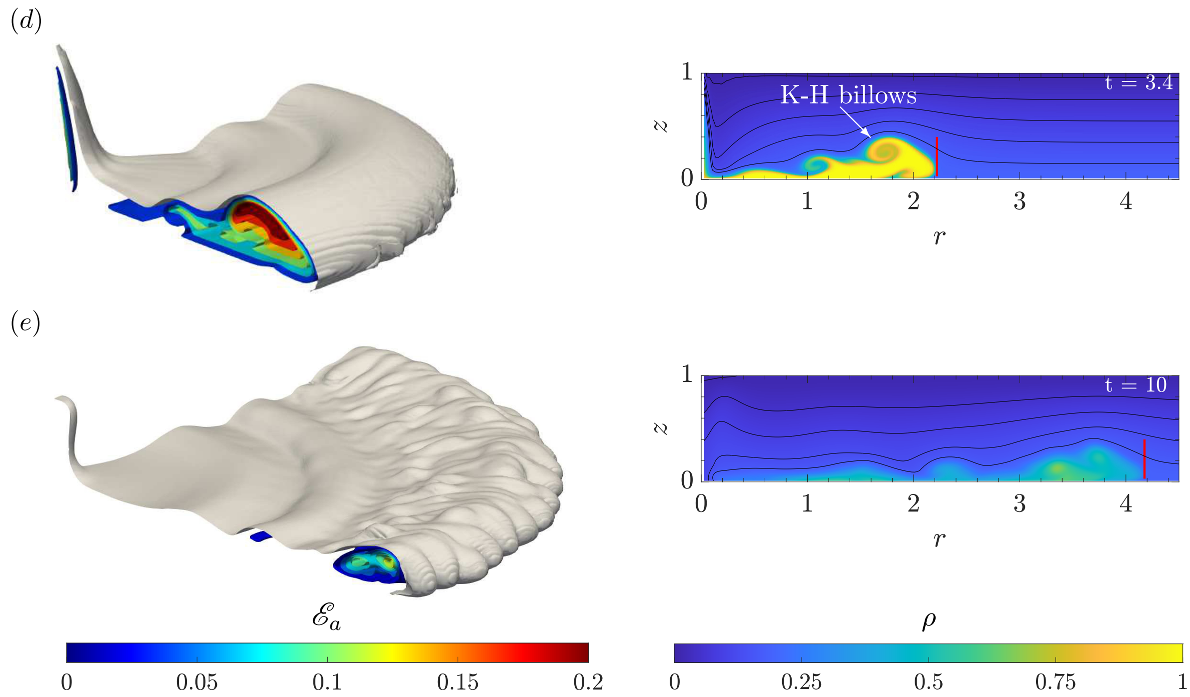

Figure 7: (Caption next page.)

the density difference between the head and the bottom wall is small, resulting in the $\mathscr{E}_a$ of the head being lower than that of the K-H billows. Therefore, the billows do not merge with the current head as observed for the $S = 0$ and $S = 0.2$ cases. Eventually, the propagation of the current in the inertial phase becomes negligible due to an insufficient density difference between the current and the ambient at the bottom wall.

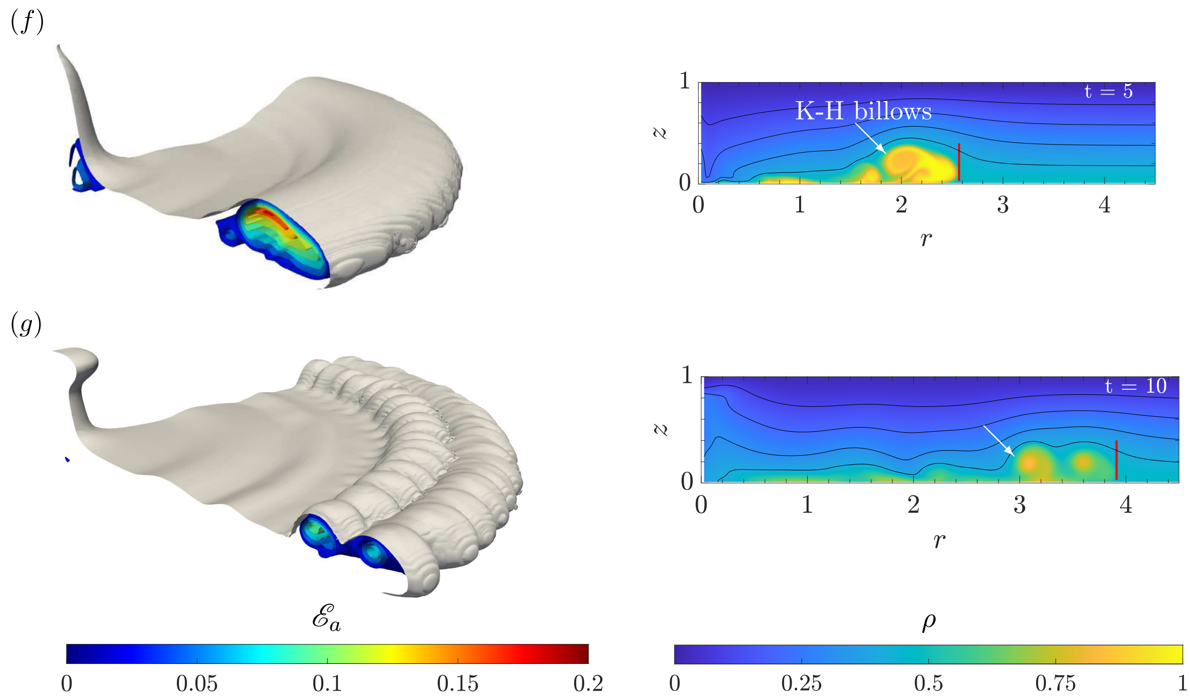

Figure 7: (Caption next page.)

For the strongly stratified case, $S = 0.8$, $\mathscr{E}_a$ attains the lowest value within the head compared to all other cases. It is worth noting that the size of the head decreases with increasing S. Similar to the $S = 0.5$

case, the tail of the current separates from the current head as the current propagates downstream, as shown in Figure 7(h). The propagation of the current becomes negligible during the slumping phase and does not transition into the inertial phase (or viscous phase) due to the insufficient density difference between the current and the ambient at the bottom wall. Consequently, gravity current flow is negligible and the behaviour may be closer to that of a strongly nonlinear solitary wave that transports mass [51]. The results of the available potential energy density show good agreement with the energy budgets.

Utilising spatial maps of local contributions to E_a, the primary region of the reversible stirring process can be identified. The effect of stratification on the energy exchange of the cylindrical gravity current is explored. With increasing stratification strength, the density difference between the current head and the bottom wall decreases. Consequently, the speed of the current further decreases, following a power law of $t^{-1/2}$ as it transitions into the inertial phase. The local Reynolds number, $Re_L = u_{f,mean}(t_{SP})H/\nu$ for $S = 0, 0.2, 0.5$ and 0.8 are 1326, 1228, 1071 and 903, respectively. For the case with $S = 0.0(0.8)$, Re_L is approximately 2.5(3.8) times smaller compared to Re fixed in the simulation. As stratification increases, Re_L decreases, leading to lower available potential energy and less turbulent flow. Strang and Fernando [52], and Peltier and Caulfield [44] have made similar observations, noting that increasing stratification reduces mixing efficiency because strongly stratified flows are less susceptible to flow instabilities.

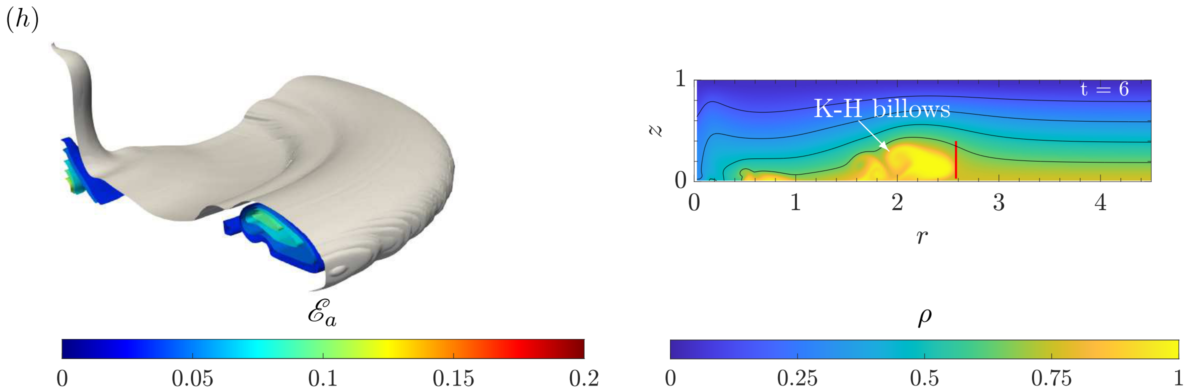

Figure 7: Time evolution of the isosurface of available potential energy density for the case with $S =$ $(a)-(c)$ 0, $(d)-(e)$ 0.2, $(f)-(g)$ 0.5 and (h) 0.8 at $Re = 3450$. The isosurface of density (or passive scalar for the stratified cases), $\rho = 0.015$ ($C = 0.015$), is plotted on top of the available potential energy density. The azimuthal-averaged density contour is plotted on the right-hand side. The white arrow indicates the Kelvin-Helmholtz billows. The solid black line represents the isopycnals.

6 Conclusion

Direct numerical simulations (DNSs) of three-dimensional cylindrical-release gravity currents in a linearly stratified ambient were conducted in this study at $Re = 3450$. The stratification strength of the ambient fluid was varied from 0 to 0.8. The main objective was to analyze the effect of stratification strength on the 'local' energy exchange of a fully cylindrical gravity current in a stratified ambient at a moderate Reynolds number. The available potential energy density, $\mathscr{E}_a$, was used to construct spatial maps of local contributions to available potential energy, E_a, and to evaluate the temporal evolution of the conversion process from available potential energy to kinetic energy through reversible stirring.

The energy budgets showed that both the kinetic energy and available potential energy of the cylindrical gravity current are affected by the ambient stratification. With increasing stratification strength, K and E_a decrease, resulting in a less energetic current observed for the strongly stratified case, $S = 0.8$. This effect is evident from the comparison of the azimuthal-averaged density contours between $S = 0$ and $S = 0.5$, where the propagation of the current is delayed by approximately one dimensionless time unit and by two dimensionless time units when S increases to 0.8. This phenomenon has also been reported in previous studies [14, 26, 19].

The investigation into 'local' energy exchanges primarily focuses on the slumping phase and the early stage of the inertial phase, during which the interaction of the Kelvin-Helmholtz billow with the current head is predominant. As the current transitions into the slumping phase, the available potential energy reaches its minimum while the kinetic energy peaks. Concurrently, the formation of the Kelvin-Helmholtz billow behind the current head occurs. The isosurfaces of $\mathscr{E}_a$ indicates that E_a is concentrated at the top part of the billow, aligning well with the temporal evolution of E_a, where there is a slight increase from a trough during the slumping phase. With increasing stratification strength, the size of the head decreases, resulting in smaller K-H billows and a decrease in $\mathscr{E}_a$.

In the inertial phase, the temporal evolution of the cylindrical gravity current behaves differently with increasing stratification strength. Merging of the K-H billows and the head is observed for unsatisfied and weakly stratified cases but not in the cases with $S \geqslant 0.5$. Besides, the tail of the current separated from the body of the current. Under the effect of stratification, the density difference between the head and the bottom wall is small, resulting in the $\mathscr{E}_a$ of the head being lower than the K-H billow and therefore the billows do not merge with the current head as observed for $S = 0$ and 0.2 cases.

The simulations conducted in this study were at a Reynolds number of $Re = 3450$ which may not represent the Reynolds number of the gravity current at every time instance. Here, the local Reynolds number, Re_L is calculated using the constant velocity during the slumping phase and ranges from $1300 < Re_L < 900$. In the inertial phase, the local Reynolds number is lower compared to the slumping phase due to the decrease in front velocity, with an exponent of $-1/2$ [26], resulting in a less energetic current. This effect is evident in the $S = 0.8$ case, where the propagation of the current becomes slower and can be negligible during the slumping phase due to the insufficient density difference between the heavy fluid and the bottom wall.

The use of available potential energy density provides detailed information about the stirring process occurring within the gravity current, where the major contribution of the energy exchange between K and E_a is now determined. These findings enhance our understanding of the dynamics of cylindrical gravity currents in stratified environments, with practical implications for natural phenomena (particle-laden [15] and multiphase flow [53]) such as the transport and mixing of pollutants and wildfire smoke. Future research could investigate the impact of varying surface area of the heavy fluid on the mixing behavior of gravity currents in stratified ambient, offering further insights for real-world applications.

Acknowledgement

This work is supported by computational resources provided by the Australian Government through Pawsey Supercomputing Centre, The University of Melbourne's Research Computing Services and the Petascale Campus Initiative. This research was supported (partially or fully) by the Australian Government through the Australian Research Council's Discovery Projects funding scheme (project DP210101965).

References

[1] J. D. Parsons. Are fast-growing martian dust storms compressible? *Geophys. Res. Lett.*, 27(15):2345–2348, 2000.

[2] B. Turnbull and J. N. McElwaine. A comparison of powder-snow avalanches at vallée de la sionne, switzerland, with plume theories. *J. Glaciol.*, 53(180):30–40, 2007.

[3] J W. Dold, A. Zinoviev, and R. O. Weber. Nonlocal flow effects in bushfire spread rates. 2006.

[4] J. E. Simpson. Gravity currents in the laboratory, atmosphere, and ocean. *Annu. Rev. Fluid Mech.*, 22(1):213–234, 1982.

[5] E. Meiburg, S. Radhakrishnan, and M. Nasr-Azadani. Modeling gravity and turbidity currents : computational approaches and challenges. *Appl. Mech. Rev.*, 67(4):040802, 2015.

[6] B. M. Marino, L. P. Thomas, and P. F. Linden. The front condition for gravity currents. *J. Fluid Mech.*, 536:49–78, 2005.

[7] H. E. Huppert and J. E. Simpson. The slumping of gravity currents. *J. Fluid Mech.*, 99(4):785–799, 1980.

[8] A. A. Alahyari and E. K. Longmire. Development and structure of a gravity current head. *Exp. Fluids*, 20(6):410–416, 1996.

[9] F. Blanchette, M. Strauss, E. Meiburg, B. Kneller, and M. E. Glinsky. High-resolution numerical simulations of resuspending gravity currents: Conditions for self-sustainment. *J. Geophys. Res. Oceans*, 110(C12):1–15, 2005.

[10] M. I. Cantero, J. R. Lee, S. Balachandar, and M. H. García. On the front velocity of gravity currents. *J. Fluid Mech.*, 586:1–39, 2007.

[11] M. I. Cantero, S. Balachandar, and M. H. García. High-resolution simulations of cylindrical density currents. *J. Fluid Mech.*, 590:437–469, 2007.
[12] M. I. Cantero, S. Balachandar, M. H. García, and D. Bock. Turbulent structures in planar gravity currents and their influence on the flow dynamics. *J. Geophys. Res. Oceans*, 113(C8):1–22, 2008.
[13] T. Maxworthy, J. Leilich, J. E. Simpson, and E. H. Meiburg. The propagation of a gravity current into a linearly stratified fluid. *J. Fluid Mech.*, 453:371–394, 2002.
[14] A. Dai, Y. L. Huang, and Y. M. Hsieh. Gravity currents propagating at the base of a linearly stratified ambient. *Phys. Fluids*, 33(6):066601, 2021.
[15] F. Necker, C. Härtel, L. Kleiser, and E. Meiburg. Mixing and dissipation in particle-driven gravity currents. *J. Fluid Mech.*, 545:339–372, 2005.
[16] V. K. Birman, J. E. Martin, and E. Meiburg. The non-boussinesq lock-exchange problem. part 2. high-resolution simulations. *J. Fluid Mech.*, 537:125–144, 2005.
[17] M. Ungarish and H. E. Huppert. Energy balances for propagating gravity currents: homogeneous and stratified ambients. *J. Fluid Mech.*, 565:363–380, 2006.
[18] M. Ungarish and H. E. Huppert. Energy balances for axisymmetric gravity currents in homogeneous and linearly stratified ambients. *J. Fluid Mech.*, 616:303–326, 2008.
[19] W. K. Lam, L. Chan, Y. Cao, D. Sutherland, R. Manasseh, K. Moinuddin, and A. Ooi. Mixing of a cylindrical gravity current in a stratified ambient. *Int. J. Heat Fluid Flow*, 107:109410, 2024.
[20] K. B. Winters, P. N. Lombard, J. J. Riley, and E. A. D'Asaro. Available potential energy and mixing in density-stratified fluids. *J. Fluid Mech.*, 289:115–128, 1995.
[21] V. K. Birman, E. Meiburg, and M. Ungarish. On gravity currents in stratified ambients. *Phys. Fluids*, 19(8):086602, 2007.
[22] W.K. Lam, L. Chan, H. Hasini, and A. Ooi. An analysis of two-dimensional stratified gravity current flow using open foam. *Int. J. Eng. Technol. (UAE)*, 7:589–595, 2018.
[23] W.K. Lam, L. Chan, H. Hasini, and A. Ooi. Direct numerical simulation of two-dimensional stratified gravity current flow with varying stratification and aspect ratio. In *21st Australasian Fluid Mechanics Conference*, pages 1–5, 2018.
[24] W. K. Lam, L. Chan, and A. Ooi. Numerical study of the dynamics of stratified gravity current. In *Proceedings of the 12th Australasian Heat and Mass Transfer Conference*, pages 1–8, 2022.
[25] W.K. Lam, L. Chan, H. Hasini, and A. Ooi. Numerical simulation of the cylindrical release gravity current in a stratified ambient. In *23rd Australasian Fluid Mechanics Conference*, pages 1–8, 2022.
[26] W. K. Lam, L. Chan, D. Sutherland, R. Manasseh, K. Moinuddin, and A. Ooi. Effect of stratification on the propagation of a cylindrical gravity current. *J. Fluid Mech.*, 983:A43, 2024.
[27] T. Zahtila, W. K Lam, Chan, L., D. Sutherland, K. Moinuddin, Dai. A., A. T. Skvortsov, R. Manasseh, and A. Ooi. On the propagation of planar gravity currents into a stratified ambient. *Phys. Fluids*, 36(3):036601, 2024.
[28] P. F. Fischer, J. W. Lottes, and S. G. Kerkemeier. nek5000 Web page, 2008.
[29] W. Lu, D. Aljubaili, T. Zahtila, L. Chan, and A. Ooi. Asymmetric wakes in flows past circular cylinders confined in channels. *J. Fluid Mech.*, 958:A8, 2023.
[30] W. Lu, Q. D. Nguyen, L. Chan, C. Lei, and A. Ooi. Flows past cylinders confined within ducts. effects of the duct width. *Int. J. Heat Fluid Flow*, 104:109208, 2023.
[31] J. Lee, L. Chan, T. Zahtila, W. Lu, G. Iaccarino, and A. Ooi. Surrogate models for multi-regime flow problems. *Phys. Rev. Fluids* (under review), 2004.
[32] J. S. Turner. *Buoyancy effects in fluids.* Cambridge University Press, Cambridge, 1979.
[33] Y. Cao, J. Philip, and A. Ooi. Characteristics of a buoyant plume in a channel with cross-flow. *Int. J. Heat Fluid Flow*, 93:108899, 2022.
[34] Y. Cao, A. Ooi, and J. Philip. Characteristics of planar buoyant jets and plumes in a turbulent channel crossflow from direct numerical simulations. *Environ. Fluid Mech.*, pages 1–28, 2024.
[35] C. Härtel, E. Meiburg, and F. Necker. Analysis and direct numerical simulation of the flow at a gravity-current head. part 1. flow topology and front speed for slip and no-slip boundaries. *J. Fluid Mech.*, 418:189–212, 2000.
[36] T. Bonometti and S. Balachandar. Effect of schmidt number on the structure and propagation of density currents. *Theor. Comput. Fluid Dyn.*, 22(5):341–361, 2008.
[37] A. Dai. High-resolution simulations of downslope gravity currents in the acceleration phase. *Phys. Fluids*, 27(7):076602, 2015.
[38] T. Zahtila, W. Lu, L. Chan, and A. Ooi. A systematic study of the grid requirements for a spectral element method solver. *Comput Fluids*, 251:105745, 2023.
[39] L. Ottolenghi, C. Adduce, R. Inghilesi, V. Armenio, and F. Roman. Entrainment and mixing in

unsteady gravity currents. *J. Hydraul. Res.*, 54(5):541–557, 2016.

[40] M. D. Patterson, C. P. Caulfield, J. N. McElwaine, and S. B. Dalziel. Time-dependent mixing in stratified kelvin-helmholtz billows: Experimental observations. *Geophys. Res. Lett.*, 33(15), 2006.

[41] A. T. Fragoso, M. D. Patterson, and J. S. Wettlaufer. Mixing in gravity currents. *J. Fluid Mech.*, 734:R2, 2013.

[42] L. Ottolenghi, C. Adduce, F. Roman, and V. Armenio. Analysis of the flow in gravity currents propagating up a slope. *Ocean Modelling*, 115:1–13, 2017.

[43] C. S. Ng, A. Ooi, and D. Chung. Potential energy in vertical natural convection. In *20th Australasian Fluid Mechanics Conference*, pages 1–4, 2016.

[44] W. R. Peltier and C. P. Caulfield. Mixing efficiency in stratified shear flows. *Annu. Rev. Fluid Mech.*, 35(1):135–167, 2003.

[45] H. Salehipour and W. R. Peltier. Diapycnal diffusivity, turbulent prandtl number and mixing efficiency in boussinesq stratified turbulence. *J. Fluid Mech.*, 775(464-500), 2015.

[46] K. B. Winters and R. Barkan. Available potential energy density for boussinesq fluid flow. *J. Fluid Mech.*, 714:476–488, 2013.

[47] D. Holliday and M. E. Mcintyre. On potential energy density in an incompressible, stratified fluid. *J. Fluid Mech.*, 107:221–225, 1981.

[48] G. Roullet and P. Klein. Available potential energy diagnosis in a direct numerical simulation of rotating stratified turbulence. *J. Fluid Mech.*, 624:45–55, 2009.

[49] J. E. Simpson. Effects of the lower boundary on the head of a gravity current. *J. Fluid Mech.*, 53(4):759–768, 1972.

[50] A. Dai and Y. L. Huang. On the merging and splitting processes in the lobe-and-cleft structure at a gravity current head. *J. Fluid Mech.*, 930:1–22, 2022.

[51] R. Manasseh, C. Ching, and H. J. S. Fernando. The transition from density-driven to wave-dominated isolated flows. *J. Fluid Mech.*, 361:253–274, 1998.

[52] E. J. Strang and H. J. S. Fernando. Entrainment and mixing in stratified shear flows. *J. Fluid Mech.*, 428(349-386), 2001.

[53] G. Cui, M. Liu, W. Dai, and Y. Gan. Pore-scale modelling of gravity-driven drainage in disordered porous media. *Int. J. Multiph. Flow*, 114:19–27, 2019.